Thermodynamics of carbon-doped Al and Ga clusters: *Ab initio* molecular dynamics simulations

Prachi Chandrachud,[1] Kavita Joshi,[2] and D. G. Kanhere[1,2]
[1]*Department of Physics, University of Pune, Ganeshkhind, Pune 411 007, India*
[2]*Centre for Modeling and Simulation, University of Pune, Ganeshkhind, Pune 411 007, India*
(Received 4 June 2007; revised manuscript received 25 August 2007; published 20 December 2007)

We have carried out extensive first principles thermodynamic simulations for Al_{13}, Ga_{13}, $Al_{12}C$, and $Ga_{12}C$. The results are based on the simulation time of 2.4 ns for each of the clusters, and the heat capacity curves have been calculated using multiple-histogram technique. Both clusters Al_{13} and Ga_{13} show higher than bulk melting temperatures. Upon doping, there is a substantial reduction in the melting temperatures of the host clusters. In the case of Ga, the carbon atom changes the geometry from decahedral to icosahedral. This change in the geometry changes the heat capacity curve significantly, making the solidlike to liquidlike transition sharper. Our results bring out the fact that an impurity can be used to tune the finite temperature properties of small clusters.

DOI: 10.1103/PhysRevB.76.235423 PACS number(s): 31.15.Ew, 31.15.Qg, 36.40.Ei, 36.40.Qv

I. INTRODUCTION

During the past decade, atomic clusters have attracted much attention due to their importance in understanding nanoscale materials.[1] It is now well established that the physical and chemical properties of such finite size systems are different from their bulk counterparts.[2] A notable example is that of the ground state geometries. The ground state geometries of most of the clusters are very different from their bulk structures. For example, a 13 atom aluminum cluster has a fivefold symmetric icosahedral structure,[3] whereas bulk aluminum forms a face centered cubic lattice. In a few cases, the nature of the bonding may be quite different from their bulk bonding, e.g., small clusters of Mg, Li-Al, and Ga show van der Waals, ionic, and covalent bonding, respectively. There is also a close relationship between structural evolution and the nature of the bonding. The shapes of the alkali atom clusters are known to follow typical jellium model predictions. However, clusters of group IV elements show significantly different evolution in their geometries because of the covalent bonding. Small clusters of Si,[4], Ge,[5] and Sn,[6] with few tens of atoms, have elongated prolate ground state geometries. Similarly, properties such as stability, ionization potential, polarizabilities, optical spectra, magnetism, etc., turn out to be different from their bulk properties.[1,2] These investigations reveal that properties of clusters are unique and do get altered, at times dramatically, depending on their size.

One of the effective ways of tuning the properties of the clusters is by adding an impurity. The magnitude of the change thus induced depends on the nature of the impurity. In many of the cases, it has been observed that a single atom can bring out significant changes in the geometry as well as in the nature of the bonding of the host cluster. The recent and very interesting example being that of metal encapsulated Si cages, where prolate geometries of small Si clusters have been transformed into small cages of Si.[7] A metalliclike bonding observed in pure Li_n clusters gets modified into a combination of ionic and metallic bonding when doped with Sn atom.[8] Thus, clusters provide a playground for tuning up the properties with the help of an appropriate impurity.

Indeed, the idea of using an impurity to alter the properties of the small clusters has been exploited by a number of works. A notable and early example is that of Al_{13}, where the well known stability of close shell systems within jellium approximation (for a total number of electrons equal to 8, 20, 28, 40, 58,…) has been exploited to enhance the stability by substituting the central Al atom with tetravalent impurities.[9–12] These studies were motivated by possibilities of using such stable clusters as building blocks for novel designer's solids. These investigations have brought out many interesting observations. Substitutional doping of an Al_{13} cluster by a tetravalent atom results in a substantial gain in the binding energy. The maximum enhancement was seen for the carbon-doped cluster, $Al_{12}C$. Interestingly, its bulk modulus turns out to be smaller than the other doped clusters. It is also observed that the behavior of the central atom is more like that of a metallic atom rather than the expected covalent behavior.

Although the ground state properties of Al_{13} and $Al_{12}X$ have been extensively probed, their finite temperature properties remain virtually unexplored. To the best of our knowledge, the only investigations reported to probe the finite temperature behavior of $Al_{12}C$ is that due to Seitsonen *et al.*[13] They found that the icosahedral structure is stable up to a temperature of the order of 930 K. Although they used *ab initio* molecular dynamics, their conclusion was based on simulations performed at only one temperature. In recent years, the finite temperature behavior of homogeneous clusters has brought out a number of interesting and unexpected features. Firstly, the measured melting temperatures turn out to be size sensitive[14,15] and, in some cases, higher than their bulk.[16] Equally interesting is the observation that even the shapes of their heat capacity curves are size sensitive.[14,17] The recent experiments on clusters of Al and Ga demonstrate that the variation in their melting temperature could be as large as 400 K over the size variation of a few atoms.[14,18]

As noted earlier, adding an impurity induces many changes in the ground state geometry, chemical bonding, and the stability of the host cluster, and hence, it is of considerable interest to probe the finite temperature behavior of such heterogeneous clusters. There have been some remarkable reports on finite temperature behavior of the mixed

clusters.[19–24] An interesting example is that of icosahedral silver nanoclusters ($N=55$ and 147), where Mottet *et al.* showed that a single impurity can considerably shift their melting temperatures.[19] Apart from altering the melting temperatures, an impurity can be used to suppress the fragmentation. For example, pure Si clusters in the size range of 15–20 atoms are known to fragment in the temperature range of 1200–1800 K.[25] It has been recently shown that these clusters could be stabilized by adding an appropriate impurity like Ti, and the fragmentation could be avoided at least until 2600 K.[23] Doping small Li clusters with Al and Sn has been shown to change the shapes of the heat capacity curves of the host clusters significantly.[22,24]

In this work, we have chosen to investigate the finite temperature properties of Al_{13}, Ga_{13}, $Al_{12}C$, and $Ga_{12}C$. Although Al_{13} and Ga_{13} are isoelectronic, they are known to exhibit very different bonding. Al clusters in this size range show delocalized charge density exhibiting metallicklike bonding, whereas small clusters of gallium are known to be covalently bonded and melt at temperatures higher than their bulk melting point. In addition, $Al_{12}C$ and $Ga_{12}C$ are 40 electron systems showing enhanced stability. Therefore, it is of considerable interest to investigate their finite temperature properties. The focus of the present work is to see the effect of doping on the heat capacity curves and to explore the correlation between their shapes and the ground state geometry. Indeed, our first principle simulations show a rather significant effect on the shape and the peak of the heat capacity, especially for Ga_{13}.

The paper is organized as follows. In Sec. II, we briefly note the computational details. Section III presents the results and discussions. First, we compare the zero temperature properties such as the ground state geometry and the nature of bonding of pure clusters to that of C-doped clusters, followed by a presentation of the finite temperature results. The paper is concluded with a summary in Sec. IV.

II. COMPUTATIONAL DETAILS

We have performed thermodynamic simulations using Born-Oppenheimer molecular dynamics based on the Kohn-Sham formulations of density functional theory.[26] The interactions between the ion and valence electrons are described using Vanderbilt's ultrasoft pseudopotentials,[27] within the generalized gradient approximation as implemented in the VASP package.[28] For Al, the energy cutoff of 9.50 Ry is used. For Ga, it is 9.54 Ry, while for C, it is 21.08 Ry. The size of the simulation box is 15 Å, which is found to provide sufficient convergence in the total electronic energy. In order to calculate the ionic heat capacities, we sample the phase space at various constant temperatures ranging from 200 to 2500 K, each with the duration of 150 ps using a Nośe thermostat.[29] Thus, the total simulation time is around 2.4 ns. We have discarded the initial 30 ps data for each temperature for the thermalization. Following the finite temperature study, the ionic heat capacity of each cluster is computed using the multiple-histogram (MH) method.[30,31] The computation of the heat capacity using the MH technique is sensitive to the number of temperatures at which the thermodynamic behavior of the cluster is simulated. The range and the number of temperatures are chosen to ensure an adequate overlap in the potential energy distribution. The method extracts the classical ionic density of states $\Omega_C(E)$ of the cluster, or equivalently, the classical ionic entropy $S(E)=k_B \ln \Omega_C(E)$, from the simulation data. With $S(E)$ in hand, one can evaluate thermodynamic averages in a variety of ensembles. The method is presented briefly in the Appendix.

Among various traditional indicators of phase change, we have calculated the root mean square bond length fluctuations (δ_{rms}) and mean square displacement (MSDs). δ_{rms} gives the average fluctuations in the bond lengths over the entire time span. For these clusters, we have calculated separate δ_{rms} for bonds between surface atoms and central atom and for bonds among surface atoms. It is defined as

$$\delta_{rms} = \frac{1}{N}\sum_{i>j} \frac{(\langle r_{ij}^2\rangle_t - \langle r_{ij}\rangle_t^2)^{1/2}}{\langle r_{ij}\rangle_t}, \tag{1}$$

where N is the number of bonds (for bonds between the surface atoms, $N=66$, and for the ones between surface atoms and central atom, $N=12$), r_{ij} is the distance between the atoms i and j, and $\langle \ldots \rangle_t$ represents a time average over the entire trajectory. The MSD for an individual atom is defined as

$$\langle \mathbf{r}_I^2(t)\rangle = \frac{1}{M}\sum_{m=1}^{M} [\mathbf{R}_I(t_{0m}+t) - \mathbf{R}_I(t_{0m})]^2, \tag{2}$$

where $\mathbf{R}_I$ is the position of the Ith atom, and we average over M different time origins t_{0m} spanning the entire trajectory. In the solidlike region, all atoms perform oscillatory motion about fixed points, resulting in a negligible mean displacement of individual atoms from their equilibrium positions. (We hold the total angular momentum of the cluster to zero, suppressing the rotation of the cluster.) In a liquidlike state, atoms diffuse throughout the cluster and the MSD eventually reaches a saturated value of the order of the square of the cluster radius. MSDs for individual atoms differentiate between a disordered cluster and an ordered cluster. A disordered cluster at low temperatures will show a spread in the MSDs of individual atoms, indicating a large variation in the displacements of different atoms in contrast to the bunching seen in MSDs for an ordered cluster. We will elaborate this while discussing the finite temperature behavior of Ga_{13} and $Ga_{12}C$. More technical details concerning the extraction of thermodynamics averages, indicators, and computation of the specific-heat curve can be found in previous work.[31]

The nature of bonding between the atoms in a cluster is analyzed using the electron localization function[32–34] (ELF) along with the total charge density and molecular orbitals. For a single determinantal wave function built from Kohn-Sham orbitals, ψ_i, the ELF is defined as[34]

$$\chi_{\mathrm{ELF}} = [1 + (D/D_h)^2]^{-1}, \tag{3}$$

where

$$D_h = (3/10)(3\pi^2)^{5/3}\rho^{5/3}, \tag{4}$$

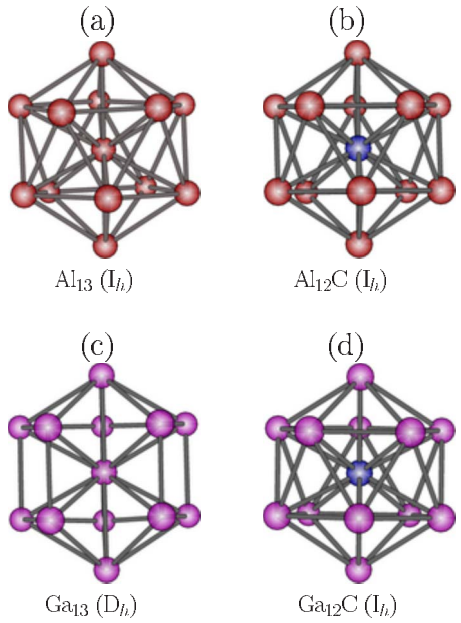

FIG. 1. (Color online) The ground state geometries of Al_{13}, $Al_{12}C$, Ga_{13}, and $Ga_{12}C$. The symbol in the bracket represents the symmetry of the cluster.

$$D = (1/2)\sum_i |\nabla\psi_i|^2 - (1/8)|\nabla\rho|^2/\rho, \tag{5}$$

with $\rho \equiv \rho(\mathbf{r})$ being the valence electron density. D is the excess local kinetic energy density due to Pauli repulsion and D_h is the Thomas-Fermi kinetic energy density. The numerical values of χ_{ELF} are conveniently normalized to a value between zero and unity. A value of 1 represents a perfect localization of the valence charge, while the value for the uniform electron gas is 0.5. Typically, the existence of an isosurface in the bonding region between two atoms at a high value of χ_{ELF}, say, ≈0.70, signifies a localized bond in that region. The ELF's can be analyzed by plotting isosurfaces which locate the localization domains. This is most conveniently done by examining the isosurfaces for successive values of ELF, starting with the highest. The locations of the maxima of ELF are called attractors and the set of all the points in space that can be connected to them by maximum gradient paths are called basins. In general, there are more that one attractor of an N-electron system, and hence, more that one basin.[35]

III. RESULTS AND DISCUSSION

We begin our discussion by examining the ground state geometries of Al_{13}, $Al_{12}C$, Ga_{13} and $Ga_{12}C$, which are shown in Fig. 1. The ground state structure of Al_{13} has already been studied and is known to be a Jahn-Teller distorted icosahedron.[36] Our geometry [Fig. 1(a)] is in agreement with the earlier results, in which the shortest bond between the central Al atom and the outer shell is 2.64 Å. It has been reported that upon the substitution by carbon, the structure changes to a perfect icosahedron with all 12 Al atoms placed at 2.53 Å from the central carbon atom.[9] Thus, the most stable structure of $Al_{12}C$ is an icosahedron with the carbon at the center [Fig. 1(b)]. The ground state geometry of Ga_{13} is known to be a slightly distorted decahedron [Fig. 1(c)], in which the distance from the central atom to surface atoms ranges from 2.69 to 2.81 Å.[37] It is interesting to note that upon doping, this decahedral structure changes to an icosahedron with the carbon atom at the center [Fig. 1(d)]. For $Ga_{12}C$, the distance from the central carbon to the outer shell is 2.53 Å. The presence of carbon shortens the bonds between the central atom and the atoms in the outer shell. Further, analysis of the various bond lengths indicates that the nearest neighbor distance between the surface atoms shows opposite trends. For $Al_{12}C$, we observe a reduction by ≈0.08 Å, while for $Ga_{12}C$, it increases by ≈0.09 Å. Table I shows relevant parameters such as the shortest bond lengths, the binding energy (BE), and the gap between the highest occupied molecular orbital and the lowest unoccupied molecular orbital (HOMO-LUMO). It can be seen that the introduction of carbon enhances the BE as well as the HOMO-LUMO gap in both clusters.

TABLE I. Some relevant parameters for the clusters investigated. Bond lengths are shown between the central atom and surface atoms.

System	Al_{13}	$Al_{12}C$	Ga_{13}	$Ga_{12}C$
Symmetry	I_h	I_h	D_h	I_h
Bond lengths (Å)	2.64–2.69	2.53	2.6–2.8	2.53
BE (eV)	−37.10	−42.30	−32.03	−37.37
HOMO-LUMO gap (eV)	1.56	2.00	1.40	2.00
Melting peak (K)	1800	900	1200	800

The nature of the bonding in all the clusters can be understood by examining the total charge density and the molecular orbitals. Jena and co-workers have extensively investigated the evolutionary character of the bonding in small Al clusters ranging from 2 to 15.[38] It has been clearly shown that the clusters with more than seven atoms show an s-p hybridized character. In contrast to this, small clusters of Ga even in the size range up to 40–45 atoms are known to be covalently bonded.[39]

In Fig. 2, we show various isosurfaces of total charge density for all the clusters. It is interesting to note that for Al_{13} [Fig. 2(a)], the charge around the central aluminum is not spherically symmetric and, in fact, shows the formation of direct bonds with six nearest neighbor Al atoms. The overall charge density is, as expected, well spread and delocalized. In contrast to this, for Ga_{13}, the formation of localized bonds is evident [Fig. 2(e)].

Significant changes are observed in the bonding due to substitution by carbon atom. For $Al_{12}C$, it can be seen that even up to 1/3 value of the charge density [Fig. 2(c)], most of the charge is around central carbon and is spherically symmetric, indicating filling of carbon centered p orbitals. Evidently, there is charge transfer from all the surface atoms towards the central carbon atom. This establishes a partial ionic bond between the central carbon atom and the surface atoms. As a consequence, the size of the cluster shrinks.

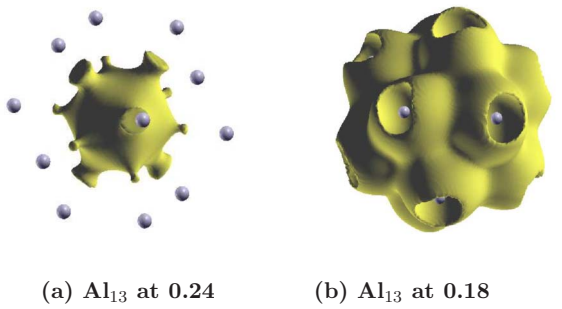

(a) Al_{13} at 0.24 (b) Al_{13} at 0.18

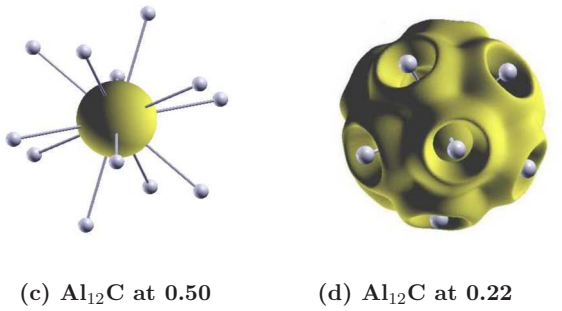

(c) $Al_{12}C$ at 0.50 (d) $Al_{12}C$ at 0.22

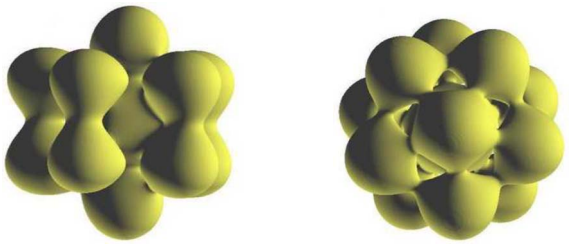

(e) Ga_{13} at 0.20 (f) $Ga_{12}C$ at 0.22

FIG. 2. (Color online) Isosurfaces of total charge density at various values for all the clusters. The values of the maximum charge density for Al_{13} and Ga_{13} are 0.26 and 0.28, respectively, while for $Al_{12}C$ and $Ga_{12}C$ are 1.50 and 1.60, respectively.

Such a charge depletion also results in a weakening of the strength of the bonds between the surface atoms. The charge density in the case of $Ga_{12}C$ shows a similar behavior. Most of the charge is around the carbon and is spherically symmetric (figure not shown). In order to understand the nature of bonding in this cluster, we show an isosurface of charge density at low value (1/7) in Fig. 2(f). This brings out the

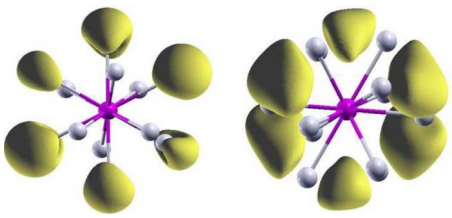

(a) $Al_{12}C$ (b) $Ga_{12}C$

FIG. 3. (Color online) Isosurfaces of charge density for the molecular orbital (HOMO-2) at about 1/4 of the maximum value.

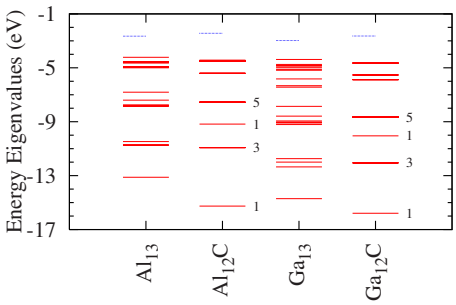

FIG. 4. (Color online) Eigenvalue spectra for all the systems. The topmost short line (blue) indicates LUMO.

localized nature of the charge in contrast to the delocalized one as seen in $Al_{12}C$.

It may be pointed out that there is a subtle difference in the molecular orbitals (MOs) participating in the bonding of the surface atoms. Figure 3 shows isosurfaces of the charge density corresponding to a typical MO (near HOMO) for both the carbon-doped clusters. The participating orbitals in $Al_{12}C$ are *s*-*p* hybridized, while in the case of $Ga_{12}C$, they are purely *p* type. The eigenvalue spectrum for all the clusters is shown in Fig. 4. The effect of introducing the impurity on the eigenvalue spectra is remarkable. In both cases, the spectra became highly degenerate, reflecting the higher symmetry of the icosahedral structure. In fact, both spectra show a jelliumlike degenerate eigenvalue structure. The lowest level is *s*-like centered around the carbon. It may be pointed out that although the spectra for both the clusters are nearly identical to that of the jellium model, there is a difference in the nature of eigenfunctions between these two clusters. In the case of $Al_{12}C$, all the eigenfunctions resemble corresponding jellium eigenfunctions of *s*, *p*, *s*, and *d* types. However, the eigenfunction of $Ga_{12}C$, especially near HOMO, is quite different and is dominantly formed by *p*-type orbitals centered on the surface Ga atoms.

So far, we have investigated the zero temperature properties of these clusters. We have observed that substitutional doping by C results in a more symmetric structure, with increased BE and higher HOMO-LUMO gap. Now, we present the results of our finite temperature simulations for pure and carbon-doped clusters. In Figs. 5 and 6, we show the ionic heat capacities of Al_{13}, $Al_{12}C$ and Ga_{13}, $Ga_{12}C$, respectively.

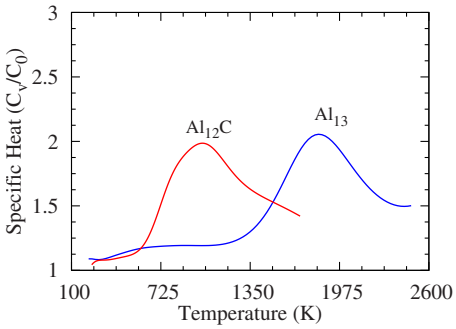

FIG. 5. (Color online) Normalized specific heat for Al_{13} and $Al_{12}C$. Note that shapes of the specific-heat curves are similar, but the melting temperature is lowered by almost 800 K upon doping.

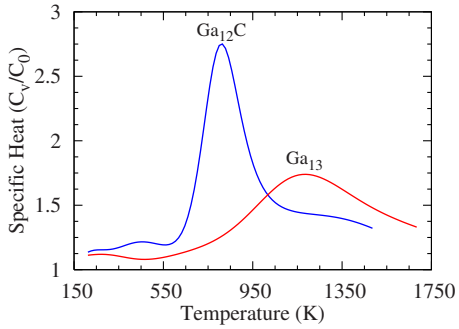

FIG. 6. (Color online) Normalized specific heat for Ga_{13} and $Ga_{12}C$. Note the significant change in the shape of the curve of $Ga_{12}C$.

In finite size systems, the solidlike to liquidlike transition is spread over a range of temperatures. The melting temperature is identified with the peak in the heat capacity curve. Several observations can be made from Figs. 5 and 6. The observed peak for Al_{13} is around 1800 K, and for Ga_{13}, it is around 1200 K. It is interesting to note that both clusters melt at substantially higher temperatures compared to their bulk counterparts, which are 933 and 303 K for Al and Ga, respectively.

The effect of carbon substitution is to decrease the melting temperature typically by ≈800 K for Al and by ≈400 K for Ga. Interestingly, both carbon-doped clusters melt in a similar temperature range, i.e., around 800–900 K. However, the most remarkable observation is the sharp nature of the specific heat curve in $Ga_{12}C$ as compared to Ga_{13}, which we shall proceed to explain.

The above noted feature can be understood in light of the change in the nature of the ground state geometry and the differences in the nature of bonding. $Ga_{12}C$ is a well ordered structure, with all 12 Ga atoms placed at a spherical shell at 2.53 Å from the center. In addition, all the nearest neighbor bond distances are the same. In contrast to this, Ga_{13} is a distorted structure with the nearest neighbor bond lengths varying between 2.57 and 2.8 Å. The manifestation of these differences can be seen in ELF as examined through their isosurfaces. We have examined the isosurfaces for these two clusters by continuously varying the isovalue, starting with the maximum (≈0.9) down to 0.55. This enables us to locate the localized regions, locations of attractors, and the connectivity of these regions. There are 13 attractors centered on the atomic sites. In Fig. 7, we show the isosurface of ELF for both Ga_{13} and $Ga_{12}C$ at the value of 0.67. This is a critical value, at which the first merging of these regions takes place for $Ga_{12}C$. The most interesting aspect is that at this value, all the regions merge and contain all the atoms. This indicates that all the surface atoms experience a similar "environment" or bond with each other with similar strength, and hence, will "melt" together. In contrast to this, Ga_{13} shows a fragmented structure [Fig. 7(a)]. The first merging of the regions establishing the connectivity is seen at a high value of ELF at 0.77. The process of merging continues as the ELF value is decreased. At a value of 0.72, we find five pairs of atoms connected to each other. This indicates that in Ga_{13} a large number of pair of atoms are strongly bonded as compared to $Ga_{12}C$. This is responsible for the higher melting temperature in this cluster. All the regions merge at a lower value of ELF ≈0.55. Figure 7 brings out this contrast and the fragmented nature of the regions. Thus, in Ga_{13}, most of the atoms experience a different environment and are bonded with the surrounding atoms with varying strength, which results in a broad transition region (or step by step bond breaking). A similar detailed analysis for Al_{13} and $Al_{12}C$ reveals that the contrast is not as significant since the symmetry remains the same in both clusters.

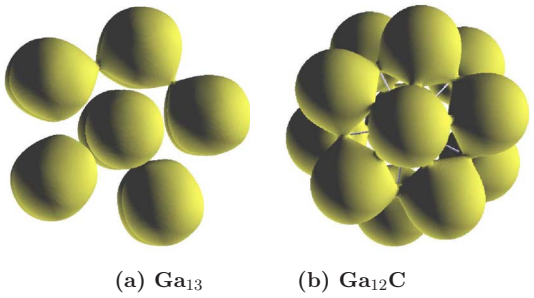

FIG. 7. (Color online) Isosurfaces of ELF for Ga_{13} and $Ga_{12}C$ at the value of 0.67.

The mean square displacements for the individual atoms bring out the difference between the Ga_{13} and $Ga_{12}C$ explicitly. Figure 8 shows MSDs for Ga_{13} and Fig. 9 for $Ga_{12}C$ at 325 K. MSDs at higher temperature show similar behavior. However, at lower temperatures, MSDs prove to be a crucial indicator distinguishing the nature of the "motion" of atoms in these two clusters. It can be seen from Figs. 8 and 9 that MSDs for Ga_{13} and $Ga_{12}C$ are significantly different at 325 K. At this temperature, there are a significant number of atoms in Ga_{13} showing considerable displacements from their "original" positions, whereas in the case of $Ga_{12}C$, all the atoms have very small values. Remarkably, the atoms having large values of MSDs in the case of Ga_{13} belong to different basins.

The dynamics of the clusters can be described by examining the trajectories of atoms at various temperatures. It is observed that around 400 K, the Al_{13} visits its first isomer, a decahedron, quite frequently. At 800 K, there is diffusive

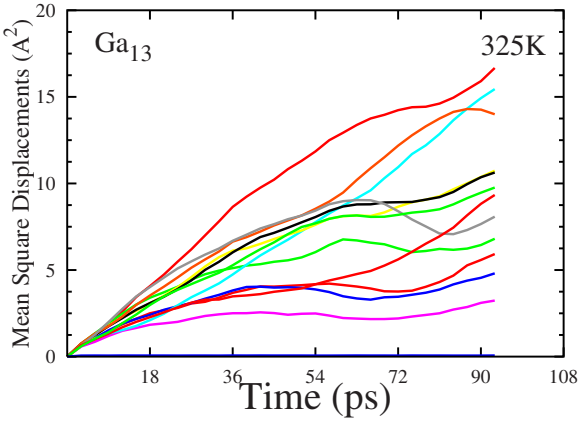

FIG. 8. (Color online) Mean square displacements for individual atoms at 325 K for Ga_{13} cluster.

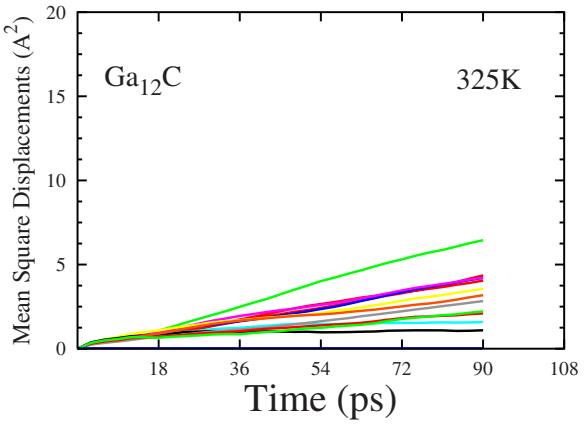

FIG. 9. (Color online) Mean square displacements for individual atoms at 325 K for $Ga_{12}C$ cluster.

motion of the surface atoms. The central aluminum atom comes out at about 1200 K, but gets replaced by other aluminum atoms, retaining the shape of the cluster. This process continues up to 1800 K, where the shell structure is completely destroyed. The peak in the heat capacity curve is associated with the destruction of the icosahedron. Ga_{13} also melts in a similar manner. It undergoes isomerization around 325 K from decahedron to icosahedron. At around 850 K, the central Ga atom comes out of the shell and gets replaced by another Ga atom. This process continues up to 1000 K. Around 1400 K, the shell structure is completely destroyed and a peak occurs in the heat capacity curve. Thus, in host (pure) clusters, the melting transition is a two step process. Isomerization is seen around 350 K, whereas the complete destruction of the shell structure is seen at a much higher temperature which is associated with the peak in the heat capacity curve. Impurity doped systems show a completely different behavior. In the case of $Al_{12}C$, there is no isomerization seen. Neither carbon atom nor surface atoms show any rigorous motion up to 700 K. Around 700 K, carbon is seen to diffuse on the surface, destroying the shell structure. Thus, the melting is a single step process. Unlike $Al_{12}C$, the surface atoms $Ga_{12}C$ show significant motion around 325 K due to the isomerization from icosahedron to decahedron. The carbon atom, however, remains at the center up to 700 K. Melting is signified by carbon diffusing to the surface, followed by destruction of the shell. Again, melting is a single step process leading to a peak around 800 K. Thus, in both doped clusters, removal of the carbon from the center initiates the melting. The above observations are substantiated by the behavior of δ_{rms} of all these clusters. We have plotted the δ_{rms} for the central atom and the average for all the surface atoms in Fig. 10. The figure clearly brings out the difference in the motion of central atom and surface atoms. For all the clusters, the central atom does not show any appreciable rise in the value of δ_{rms}. Around 400 K and above, all the clusters except for $Al_{12}C$ show distinct movements of surface atoms, which are due to the isomerization observed around that temperature.

Finally, we note an interesting aspect of our results. Although the carbon-doped clusters have higher BE (≈5 eV),

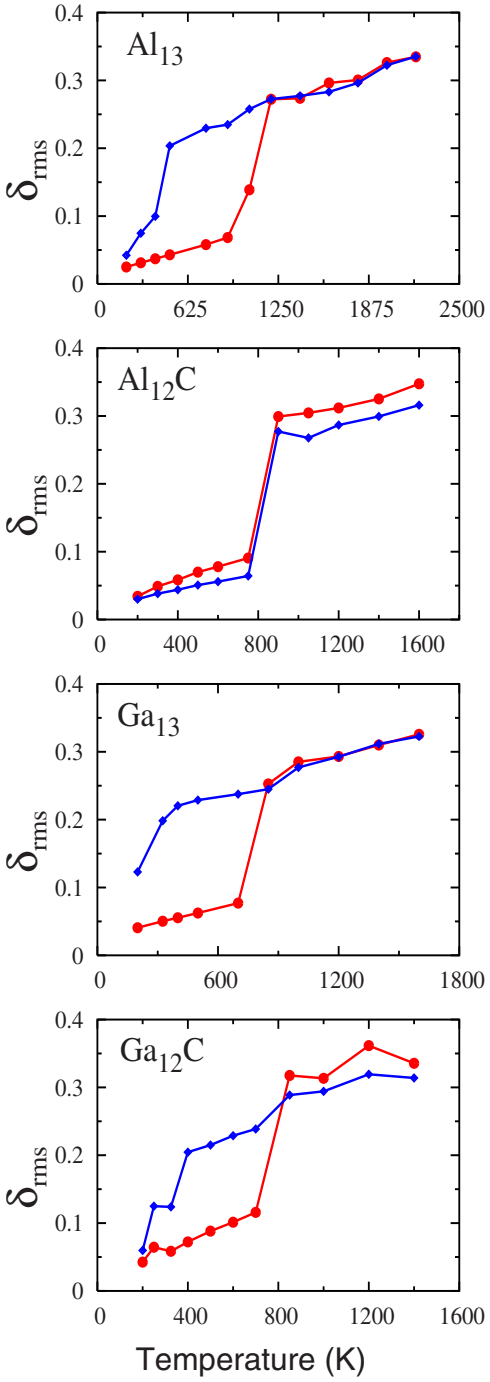

FIG. 10. (Color online) δ_{rms} for surface atoms (filled circles, blue) and central atom (filled diamonds, red) for all the clusters averaged over 90 ps.

they melt at much lower temperatures. The enhanced BE is due to the complete filling of fivefold degenerate HOMO due to the addition of an extra electron, an effect observed not only for carbon but also for other tetravalent elements such as Si, Ge, Sn, etc.[10,11] However, substitution of carbon at the center weakens the bonds between surface atoms. This initiates the melting process at much lower temperature. It may also be pointed out that BE is a measure of complete dissociation, while the process of melting does not change the number of electrons, retaining the close shell property.

IV. SUMMARY

We have carried out extensive first principle thermodynamics simulations for Al_{13} and Ga_{13} with and without substitution by C. Our results clearly show that for both clusters, there is a substantial reduction in the melting temperature of host clusters. A single C atom is seen to induce a substantial change in the shape of the heat capacity curve in the case of Ga. In a sense, $Ga_{12}C$ shows a much sharper transition. It is interesting to note that this small size cluster shows such a sharp transition when most of the homogeneous clusters in this size range show a very broad melting transition. Finally, we note that the binding energy of the carbon-doped clusters, as noted in Table I, is higher by about 5 eV. However, their melting temperatures are lower than the corresponding host clusters.

ACKNOWLEDGMENTS

K.J. and D.G.K. thank the Indo French Center for the Promotion of Advanced Research (IFCPAR) for partial financial support (Grant No. 3104-2). The authors also thank M.-S. Lee and S. Krishnamurty for many useful discussions.

APPENDIX

The multiple-histogram (MH) method is a technique that permits a better estimation of the classical density of states from the discrete sampling of potential energy. The method permits a separate treatment of the configurational and kinetic parts of the problem. This separation is advantageous, because the kinetic part of the problem can be handled analytically and the sampling is required only for the potential energy over the configuration space.

The first step in extracting $\Omega_C(E)$ is to construct a histogram of the potential energy at each of the τ temperatures used for the sampling runs. For this purpose, the potential energy scale, which ranges from V_0 to some maximum observed value $V_{\max}$, is divided into N_V intervals (or *bins*) of width $\delta V=(V_{\max}-V_0)/N_V$. The same bins should be used for all temperatures. We shall denote each temperature by an index i satisfying $1\leq i\leq \tau$, and each bin by an index j satisfying $1\leq j\leq N_V$, with V_j the central value of the potential energy in the jth bin. Let n_{ij} be the number of times the potential energy assumes a value lying in the jth bin at a temperature i. Then the probability that the system takes a potential energy in the jth bin at an inverse temperature $\beta_i = 1/k_B T_i$ is estimated from the simulation as

$$p_{ij}^{\text{sim}} = \frac{n_{ij}}{\sum_j n_{ij}}. \tag{A1}$$

On the other hand, in the canonical ensemble, the probability of finding a cluster with potential energy Vj is given by

$$p_{ij} = p(V_j, T_i) = \frac{\Omega_C(V_j)\exp(-\beta_i V_j)}{Z_C(\beta_i)}, \tag{A2}$$

where Z_C is the partition function and $\Omega_C(E)$ is the density of states. Equating p_{ij}^{sim} and p_{ij} and taking logarithms, we get

$$\frac{S_j}{k_B} + \alpha_i = \beta_i V_j + \ln n_{ij}, \tag{A3}$$

where

$$S_j = \ln[\Omega_C(V_j)], \tag{A4}$$

$$\alpha_i = \ln\left(\sum_j n_{ij}\right) - \ln Z_C(\beta_i). \tag{A5}$$

For each i and j, this results in $N_\tau \times N_V$ equations which must be solved for S_j and Z_i $[=Z_C(\beta_i)]$. This is done by minimizing (least square fit),

$$\sum_{i,j} n_{ij}\left[\frac{S_j}{k_B} + \ln\left(\sum_j n_{ij}\right) - \ln Z_i - \beta_i V_j - \ln n_{ij}\right]^2. \tag{A6}$$

This simplifies to a system of N_τ equations with N_τ unknown parameters. After eliminating S_j, we get

$$\alpha_i\left(\sum_{j=1}^{N_v} n_{ij}\right)\sum_{i'=1}^{N_\tau}\left[\sum_{j=1}^{N_v}\frac{n_{ij}n_{i''j}\alpha_{i'}}{\sum_{i''=1}^{N_\tau} n_{i''j}}\right] = \sum_{j=1}^{N_v}\left\{n_{ij}(\ln n_{ij} + \beta_i V_j) - \sum_{i'=1}^{N_\tau}\left[\frac{n_{ij}n_{i'j}(\ln n_{i'j} + \beta_{i'} V_j)}{\sum_{i''=1}^{N_\tau} n_{i''j}}\right]\right\}. \tag{A7}$$

We have used the Gauss elimination method to solve the above equations. Since the equations are overdetermined, the α_i that are obtained are relative to one of them. Since our temperatures are ordered in ascending order, choosing $\alpha_0 = 0$ corresponds to the choice of entropy reference. The parameters α_i then enable us to compute the entropy S_j, the partition function $Z(\beta_i)$, the internal energy $U(T)$, and the configurational specific heat C_v as follows:

$$S_j = k_B\frac{\sum_{i=1}^{N_\tau} n_{ij}(\ln n_{ij} + \beta_i V_j - \alpha_i)}{\sum_{i=1}^{N_\tau} n_{ij}}, \tag{A8}$$

$$Z(T) = \sum_{j=1}^{N_v}\exp\left(S_j - \frac{V_j}{T}\right), \tag{A9}$$

$$U(T) = \frac{3T(N-1)}{2} + \frac{1}{Z}\sum_{j=1}^{N_v}\exp\left(S_j - \frac{V_j}{T}\right)V_j, \tag{A10}$$

$$C_v = \frac{3(N-1)}{2} + \frac{1}{T^2}(\langle V^2\rangle - \langle V\rangle^2), \tag{A11}$$

where $\langle V\rangle = U(T)$. It may be noted that because of the use of a least square fit [Eqs. (A6) and (A7)], the resulting specific-heat curves are smooth. We estimate the error in the melting temperature to be of the order of 25 K.

[1] *Physics and Chemistry of Finite Systems: From Clusters to Crystals*, edited by P. Jena, S. N. Khanna, and B. K. Rao (Kluwer Academic, Dordrecht, 1992), Vols. 1 and 2; *Clusters and Nanostructured Materials*, edited by P. Jena and S. N. Behera (Nova Science, New York, 1996).

[2] Vijay Kumar, E. Esfarjini, and Y. Kawazoe, *Advances in Cluster Science* (Springer-Verlag, Heidelberg, 2000); *Clusters of Atoms and Molecules I and II: Theory, Experiment, and Clusters of Atoms*, edited by H. Haberland (Springer-Verlag, Berlin, 1994).

[3] U. Röthlisberger, W. Andreoni, and P. Giannozzi, J. Chem. Phys. **96**, 1248 (1992).

[4] M. F. Jarrold and V. A. Constant, Phys. Rev. Lett. **67**, 2994 (1991); M. F. Jarrold and J. E. Bower, J. Chem. Phys. **96**, 9180 (1992).

[5] J. M. Hunter, J. L. Fye, M. F. Jarrold, and J. E. Bower, Phys. Rev. Lett. **73**, 2063 (1994).

[6] A. A. Shvartsburg and M. F. Jarrold, Phys. Rev. A **60**, 1235 (1999).

[7] H. Hiura, T. Miyazaki, and T. Kanayama, Phys. Rev. Lett. **86**, 1733 (2001).

[8] M.-S. Lee, D. G. Kanhere, and K. Joshi, Phys. Rev. A **72**, 015201 (2005).

[9] S. N. Khanna and P. Jena, Phys. Rev. Lett. **69**, 1664 (1992).

[10] X. G. Gong and V. Kumar, Phys. Rev. Lett. **70**, 2078 (1993).

[11] V. Kumar and V. Sundararajan, Phys. Rev. B **57**, 4939 (1998).

[12] S. F. Li and X. G. Gong, Phys. Rev. B **70**, 075404 (2004); **74**, 045432 (2006).

[13] A. P. Seitsonen, K. Laasonen, R. M. Nieminen, and M. L. Klein, J. Chem. Phys. **103**, 8075 (1995).

[14] G. A. Breaux, D. A. Hillman, C. M. Neal, R. C. Benirschke, and M. F. Jarrold, J. Am. Chem. Soc. **126**, 8628 (2004).

[15] A. Aguado and J. M. Lopez, Phys. Rev. Lett. **94**, 233401 (2005); M. Schmidt, R. Kusche, B. Issendorff, and H. Haberland, Nature (London) **393**, 238 (1998).

[16] G. A. Breaux, R. C. Benirschke, T. Sugai, B. S. Kinnear, and M. F. Jarrold, Phys. Rev. Lett. **91**, 215508 (2003).

[17] K. Joshi, S. Krishnamurty, and D. G. Kanhere, Phys. Rev. Lett. **96**, 135703 (2006).

[18] G. A. Breaux, C. M. Neal, B. Cao, and M. F. Jarrold, Phys. Rev. Lett. **94**, 173401 (2005).

[19] C. Mottet, G. Rossi, F. Baletto, and R. Ferrando, Phys. Rev. Lett. **95**, 035501 (2005).

[20] A. Aguado, L. E. González, and J. M. López, J. Phys. Chem. B **108**, 11722 (2004).

[21] D. Cheng, S. Huang, and W. Wang, Phys. Rev. B **74**, 064117 (2006).

[22] M.-S. Lee, S. Gowtham, H. He, K.-C. Lau, L. Pan, and D. G. Kanhere, Phys. Rev. B **74**, 245412 (2006).

[23] S. Zorriasatein, K. Joshi, and D. G. Kanhere, Phys. Rev. B **75**, 045117 (2007).

[24] K. Joshi and D. G. Kanhere, J. Chem. Phys. **119**, 12301 (2003).

[25] S. Krishnamurty, K. Joshi, D. G. Kanhere, and S. A. Blundell, Phys. Rev. B **73**, 045419 (2006).

[26] M. C. Payne, M. P. Teter, D. C. Allen, T. A. Arias, and J. D. Joannopoulos, Rev. Mod. Phys. **64**, 1045 (1992).

[27] D. Vanderbilt, Phys. Rev. B **41**, 7892 (1990).

[28] Vienna *ab initio* simulation package (Technische Universität Wien, 1999); G. Kresse and J. Furthmüller, Phys. Rev. B **54**, 11169 (1996).

[29] S. Nośe, Mol. Phys. **52**, 255 (1984).

[30] A. M. Ferrenberg and R. H. Swendsen, Phys. Rev. Lett. **61**, 2635 (1988); P. Labastie and R. L. Whetten, *ibid.* **65**, 1567 (1990).

[31] D. G. Kanhere, A. Vichare, and S. A. Blundell, *Reviews in Modern Quantum Chemistry*, edited by K. D. Sen (World Scientific, Singapore, 2001).

[32] B. Silvi and A. Savin, Nature (London) **371**, 683 (1994).

[33] R. Rousseau and D. Marx, Chem.-Eur. J. **6**, 2982 (2000); Phys. Rev. Lett. **80**, 2574 (1998); J. Chem. Phys. **111**, 5091 (1999); Chem. Phys. Lett. **295**, 41 (1998).

[34] A. D. Becke and K. E. Edgecombe, J. Chem. Phys. **92**, 5397 (1990).

[35] D. Marx and A. Savin, Angew. Chem. **109**, 2168 (1997); Angew. Chem., Int. Ed. Engl. **36**, 2077 (1997).

[36] H.-P. Cheng, R. S. Berry, and R. L. Whetten, Phys. Rev. B **43**, 10647 (1991); B. K. Rao, S. N. Khanna, and P. Jena, *ibid.* **62**, 4666 (2000).

[37] J.-Y. Yi, Phys. Rev. B **61**, 7277 (2000).

[38] S. N. Khanna and P. Jena, Phys. Rev. B **51**, 13705 (1995); X. Li, H. Wu, X.-B. Wang, and L.-S. Wang, Phys. Rev. Lett. **81**, 1909 (1998); B. K. Rao and P. Jena, J. Chem. Phys. **111**, 1890 (1999).

[39] S. Krishnamurty, K. Joshi, S. Zorriasatein, and D. G. Kanhere, J. Chem. Phys. **127**, 054308 (2007).